SERS and DFT study of water on metal cathodes of silver, gold and platinum nanoparticles

Jian-Feng Li, Yi-Fan Huang, Sai Duan, Ran Pang, De-Yin Wu,* Bin Ren, Xin Xu and Zhong-Qun Tian

Received 16th September 2009, Accepted 23rd December 2009
First published as an Advance Article on the web 26th January 2010
DOI: 10.1039/b919266b

The observed surface-enhanced Raman scattering (SERS) spectra of water adsorbed on metal film electrodes of silver, gold, and platinum nanoparticles were used to infer interfacial water structures on the basis of the change of the electrochemical vibrational Stark tuning rates and the relative Raman intensity of the stretching and bending modes. To explain the increase of the relative Raman intensity ratio of the bending and stretching vibrations at the very negative potential region, density functional theory calculations provide the conceptual model. The specific enhancement effect for the bending mode was closely associated with the water adsorption structure in a hydrogen bonded configuration through its H-end binding to surface sites with large polarizability due to strong cathodic polarization. The present results allow us to propose that interfacial water molecules exist on these metal cathodes with different hydrogen bonding interactions, *i.e.*, the HO–H···H–Pt dihydrogen bond for platinum and the HO–H···Ag(Au) for silver and gold. This dihydrogen bonding configuration on platinum is further supported from observation of the Pt–H stretching band. Furthermore, the influences of the pH effect on SERS intensity and vibrational Stark effect on the gold electrode indicate that the O–H stretching SERS signals are enhanced in the alkaline solutions because of the hydrated hydroxide surface species adsorbed on the gold cathode.

Introduction

The physical and chemical properties of water molecules adjacent to metal surfaces are affected remarkably by metal substrates. This is of special interest in many aspects; not only electrochemistry, but also biology and physics. As an important solvent molecule, the structure and orientation of water adsorbed on the metal electrode surface can directly affect electrochemical reactions in electrode/aqueous solution interfaces under experimental conditions, such as potential polarization, light irradiation, or high energy electron beams and so on.[1–4] In these cases, there exist various surface species, such as unsaturated hydrogen-bonded water, protonated water, hydrated hydrogen atoms, hydrated electrons, and hydrated hydroxide ions. They are not only unstable species with a limited lifetime but also have strong chemical activity. Unfortunately, detailed information on water molecules lodged in the interface gained by conventional electrochemical methods has not been straightforward and free of questions.[5,6] Therefore, clarifying the structure and orientation of interfacial water at a microscopic level can greatly improve our fundamental understanding of the electrode/electrolyte interface, which is an eternal issue in electrochemistry so far.

State Key Laboratory of Physical Chemistry of Solid Surfaces and College of Chemistry and Chemical Engineering, Xiamen University, Xiamen, 361005, Fujian, China. E-mail: dywu@xmu.edu.cn; Fax: 86-592-2186979; Tel: 86-5922189023

A variety of *in situ* spectroscopic techniques have provided new information about the microscopic structure and dynamics of water molecules at the molecular level in metal interfaces.[4,7–13] It is worth noting that interfacial water molecules have been characterized in many coadsorption systems containing anions or neutral molecules.[14,15] These studies mainly focused on the vibrational spectra of interfacial water in the range of the potential close to the potential of zero charge (PZC), where the interaction between water and electrodes is relatively weak. However, when the applied potential is further moved negatively, the interaction of water with the electrode surface becomes strong, and depends on the applied potential, the electrode materials, and the solution pH. In the potential region of the severe hydrogen evolution reaction (HER), a detailed insight on interfacial water has remained elusive.

Surface-enhanced Raman spectroscopy (SERS) had been considered as a highly sensitive tool for investigating vibrational characteristics of interfacial water, not only avoiding extensive interference from the bulk water but also tremendously enhancing the Raman signals of surface molecules.[16–23] Furthermore, all these studies are limited to the rough electrodes of bulk coinage metals (*i.e.*, silver, gold, and copper), which are known to exhibit a large surface enhancement factor up to 10^6 or more.[24–26] However, it is still difficult to observe SERS of water adsorbed on transition metal electrodes, which is widely accepted to play an important role in electrocatalytic activity.

Recently, our group demonstrated that the SERS signals of interfacial water molecules could be observed from the film

electrodes of not only gold nanoparticles, but also transition metal nanoparticles.[27] Although nanoscale rough transition metals (VIII B group elements) of practical and fundamental importance can directly generate SERS activities, the interband excitation appears in the whole region of visible light so that the relatively low SERS enhancement effect on pure transition metals can be observed.[28,29] To improve the enhancement effect of transition-metal systems, Tian's group developed a method to synthesize gold core transition-metal (*e.g.*, Pt, Pd, and Rh) shell nanoparticles in order to "borrow" the SERS activity of the Au core.[30] Generally, several chemically coated layers (*ca.* 1–5 atomic layers) of a transition metal on highly SERS-active Au nanoparticles exhibit about a two-order enhancement effect compared to that of the same adsorbed species on pure transition metal surfaces. Therefore, their SERS signals can be significantly enhanced in comparison to those from pure transition metal nanoparticles. This strategy is appreciably advantageous to investigate some molecules with a low Raman cross section that were impractical to study in the past. It allows us to obtain the Raman spectra of interfacial water, which has a small Raman cross-section, on transition metals of Pt and Pd.[27] Note that these core–shell nanoparticles have the chemical properties of the shell but show the enhancement provided by surface plasmon resonance of the gold core.

In this report we have two goals. First, we present SERS of water on film electrodes of silver, gold, and platinum nanoparticles in the HER potential region. Since there is a special d orbital characteristic of platinum, the Pt–H bond is the strongest and the most stable among the three metals so that its SERS signal can be also observed together with interfacial water.[31] The hydrogen bonding interaction, the pH effect and the potential effect will be analyzed in this section. Second, the density functional theory (DFT) approach is used to determine the adsorption structure and to interpret the relative Raman intensities of the bending and stretching modes of interfacial water. Combined with DFT calculations, the SERS spectra obtained allows us to scrutinize the interfacial structure of water on these metal surfaces.

Experimental

Preparation of film electrodes of nanoparticles

We first synthesized, respectively, silver and gold particles according to the sophisticated Frens' method.[32] The silver nanoparticles were prepared through the reduction of a 200 ml 1 mM $AgNO_3$ solution using 6 ml 1% wt sodium citrate. For synthesis of gold nanoparticles, the chemical 200 ml 0.01% wt $HAuCl_4$ solution was reduced by 1.4 ml 1% wt sodium citrate under boiling water. Their spherical particle diameters were $\sim$75 nm for silver and $\sim$55 nm for gold, which are determined by transmission electron microscope. Then the gold nanoparticles were further used as cores, onto which 4–5 monolayers (corresponding to around 1.4 nm) of platinum were coated to form core–shell nanoparticles. The Au@Pt nanoparticle sol was prepared according to the protocol previously reported.[27] The thickness of the Pt shell was controlled simply through changing the amount of H_2PtCl_6 to Au sols. After several rounds of cleaning and concentration by centrifugation, pure silver and gold nanoparticles and Au@Pt core–shell nanoparticles were placed and fully covered on their smooth metal electrode surfaces, respectively, and then dried in vacuum. Henceforth, Pt represents an Au@Pt core–shell nanoparticle modified electrode.

Raman measurements

The potential-dependent SERS spectra were measured by using Dilor LabRaman I on silver, gold, and platinum electrodes in 0.1 M $NaClO_4$ solution. Here, two light gratings were used to record the SERS spectra at the low and high spectral resolutions with 300 lines mm^{-1} and 1800 lines mm^{-1}, respectively. The experimental potential region is more negative than the PZC potentials, which for the metals in bulk are about -0.9 V (Ag),[33] 0.2–0.3 V (Au),[33] and 0.2 V (Pt)[34] *versus* a saturated calomel electrode (SCE), respectively. The excitation line of 632.8 nm used was selected to avoid the significant damping of surface plasmon resonance from the interband excitation of gold nanoparticles.[35,36] The electrochemical cell used to measure Raman spectra was home made. The applied potential extends to -2.0 V *vs.* SCE. After considering the Ohmic drop this is corrected to about -1.9 V.

Results and discussion

SERS spectra of water on film electrodes of nanoparticles

Fig. 1 presents the whole SERS spectra of water adsorbed on the film electrodes of silver and gold nanoparticles. The SERS spectra are recorded with the 300 lines mm^{-1} light grating at low spectral resolution. In the two SERS spectra, there exist very strong background profiles, which were interpreted due to the emission of the electron-hole pair excitation on SERS active metal surfaces.[17,37,38] For the silver electrode, the maximum of the background spectra appears at about 540 cm^{-1} at -0.4 V, which is closer to the Rayleigh scattering line than the value of 860 cm^{-1} found at the same potential for the gold film electrode. The intensity of the emission profile is in general used to measure the SERS activity of the metal substrate.[37] With negatively moving potentials, the peaks of the background profiles shift dependent on the metal electrodes. As seen in Fig. 1, the opposite trends can be observed for the silver and gold electrodes.

By inspecting Fig. 1a, it can be found that the Raman bands observed at 470, 1600, and 3450 cm^{-1} become stronger for water adsorbed on the silver film electrode as the potential moves negatively from -1.2 V to -1.9 V. These bands were attributed to the libration, bending and OH stretching vibrations of water.[21,23] Fig. 1a showed that a wide band at 2770–2940 cm^{-1} (the band centre at 2840 cm^{-1}) appeared as the relative positive potential becomes weaker and finally disappears with negatively moving potential.

On the gold film electrode, three intense Raman bands were observed at 590, 1620, and 3450 cm^{-1}, which can be also attributed to the libration, bending, and stretching vibrations of water, respectively. Their signal and noise ratios are better than that observed in a roughed gold electrode in bulk.[23] The peak of the OH stretching band has a significant red shift with

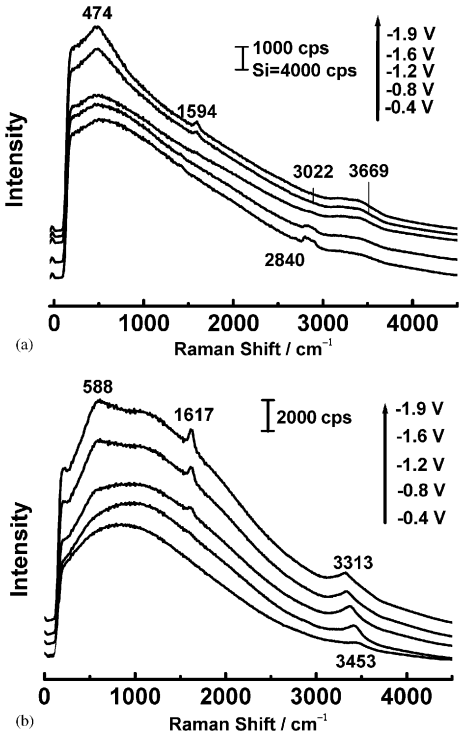

Fig. 1 Whole SERS spectra of interfacial water on film electrodes of silver (a) and gold (b) nanoparticles with the sizes of ~75 nm and ~55 nm under the excitation line 632.8 nm in aqueous solution (0.1 M $NaClO_4$).

negatively moving potential. Meanwhile, as observed on the silver film electrode, the intensities of these bands increased.

The O–H stretching vibrations

To further check the electrochemical potential effect on the SERS vibrational bands of water, the 1800 lines mm^{-1} light grating was used to record the Raman scattering light. After background subtraction, the potential-dependent SERS spectra are presented in Fig. 2. The observed frequencies are presented in Table 1. The strong potential-dependence in the spectral frequency and intensity clearly demonstrates that the characteristics of these signals must be derived from the surface water molecules, not from the bulk water. The intense Raman bands in bulk water were observed at 1641 cm^{-1} for the bending mode and at 3224 and 3434 cm^{-1} for the O–H stretching vibrations.[29]

Fig. 3 shows the vibrational Stark effect of the O–H stretching vibration that measures the extent of the frequency shift with applied potential. The Stark effect was also shown in Fig. 3 for the O–H stretching frequencies varying with the potential on Au@Pd (labelled Pd).[27] It is worth noting that the frequency shift of the O–H vibrations is larger on Au than that on Ag and Pt, indicating that the frequency shift is very sensitive to the electrode materials. From Fig. 3, the Stark tuning rate was estimated to be about 80 cm^{-1} V^{-1} on Au, which is larger than 14, 30, and 76 cm^{-1} V^{-1} for Pt, Ag, and Pd,[27] respectively. As seen in Fig. 3, the Stark tuning rate on Pt is the smallest.

For these electrode interfaces the electric fields in the double electric layer should be similar each other due to the similar shape and size of the nanoparticles as well as in the same concentration of electrolytes. Therefore, the difference in the Stark effect may arise from the two factors, the hydrogen bonding interaction between water molecules and the water-electrode bonding interaction.

The induced red shift of the hydrogen bond on the O–H vibrational frequency have extensively investigated in water.[39,40] From these different suggested assignments, the O–H stretching frequency is decreased depending on the number of hydrogen-bond formed.[41] As shown in Table 1, the Raman bands of water vapor in the O–H stretching region are 3657 and 3756 cm^{-1},[42] whereas the band at around 3220 cm^{-1} in the ice and liquid water was assigned to a water molecule perfectly binding to four neighboring water molecules through the hydrogen bonds.[41] For bulk water, the vibrational frequencies for the Raman bands of the O–H stretching vibrations are 3232 and 3437 cm^{-1} in pure water[39] and 3224 and 3434 cm^{-1} in 0.1 M $NaClO_4$.[27] The latter bands at 3437 cm^{-1} should correspond to a number of hydrogen bonds higher than that of the band at 3520 cm^{-1}, but their number of hydrogen bonds should be less than four.

Interaction between water and metal surfaces can cause the redshift of O–H stretching frequencies. The negative surface charge favors the binding of the H-end of water to the electrode surface,[43,44] forming the O–H···M hydrogen bond. The HB O–H vibrational frequencies may significantly red-shift when water binds to metal surfaces through the abnormal hydrogen bond, HO–H···M.[45–47] In this case, the charge transfer takes place from metal atoms to the antibonding orbital of the O–H bond, weakening the O–H bond and decreasing its stretching frequencies. On metal electrodes, it is expected that the more negative the potential of the PZC and the stronger the hydrogen bond, the more significant a red shift should be observed.[10,44,45] In the present work, the large Stark tuning rate of the O–H stretching vibration on Au indicates that the interaction plays an important role. The PZC potential for a gold electrode is ~0.2 V, whereas for the silver electrode it is about −0.9 V. Therefore, a small Stark tuning rate was observed on the silver film electrode due to the small potential difference from its PZC potential. However, for the platinum electrode, the smallest Stark tuning rate is due to water adsorption at the second layer above the first surface hydrogen adsorption layer.[27] This causes the vibrational frequency shift to be insensitive to a change in applied electrode potential.

HOH bending vibrations

The SERS band of the water bending mode was observed at 1609, 1620, and 1616 cm^{-1} for Ag, Au, and Pt electrodes, respectively. For all the three metal electrodes the Stark tuning rates of these bending bands are very small, less than 3 cm^{-1} V^{-1}. The previous study suggested the existence of two overlapping Raman bands (the main peak at 1645 cm^{-1} and the shoulder peak at 1625 cm^{-1}) for bending vibrations of liquid water.[39] The lower-frequency component of the bending bands was attributed to the partially hydrogen-bonded water, while the higher-frequency component was assigned to fully hydrogen-bonded water.[48] The present values in Fig. 2 locate between

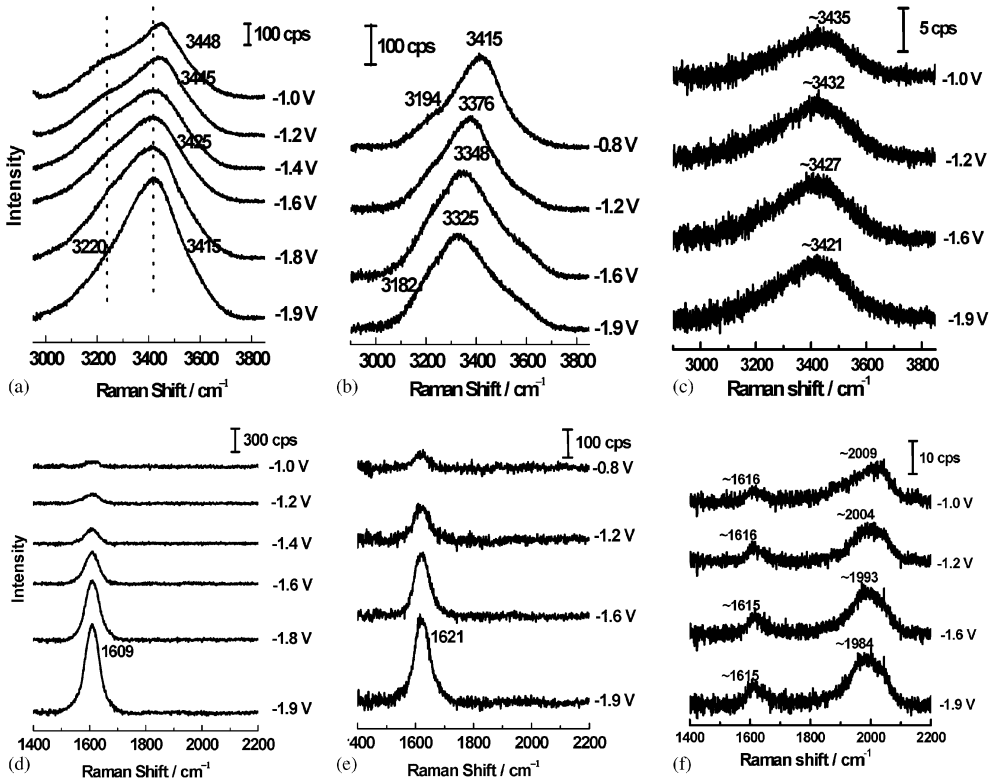

Fig. 2 High resolution SERS spectra of water adsorbed on film electrodes of silver, gold, and platinum nanoparticles at potentials negative to the PZC potential with respect to the SCE. (a), (b), and (c) are SERS spectra of the O–H stretching vibrations on silver, gold, and platinum; (d), (e), and (f) are SERS spectra of the HOH bending vibrations on silver, gold, and platinum.

Table 1 Vibrational frequencies (cm^{-1}) and assignments of vibrational bands of free water, pure liquid water, and interfacial water molecules

	Raman[a]	Raman[b]	SERS[c]			
Symbols	Gas	Pure liquid	−1.6 V/Ag	−1.2 V/Au	−1.2 V/Pt	Assignments
ν_1	1595	1610	1608	1612	1616	HOH bend
ν_2		1643				HOH bend
ν_3		3232(3224)	(3229)	(3239)	(3283)	O–H stretch
ν_4		3437(3434)	3440(3433)	3384(3376)	3432(3438)	O–H stretch
ν_5	3657	3520	(3556)	(3481)		O–H stretch
ν_6	3756					O–H stretch

[a] Free water molecule in gas phases from ref. 52 and 53. [b] Pure water, from ref. 48. The Raman bands observed in 0.1 M $NaClO_4$ aqueous solutions are presented in parenthesis from Ref. 27. [c] The vibrational frequencies in the parenthesis are obtained by modeling the observed Raman spectra as a sum of n Lorentz-type functions.

the lower-frequency component and the bending frequency of 1595 cm^{-1} for water in the gas phase, indicating that the interfacial water belongs to a low-coordinated hydrogen bonding water contributing to the SERS. Meanwhile, the weak water–metal hydrogen bonding interaction should lead to a blueshift of the bending mode.[46] Recently, the lower bending band around 1600–1620 cm^{-1} was observed in surface-enhanced infrared spectra of water on a CO-coated platinum electrode and halide anionic coadsorption systems on gold electrodes.[13,49]

A very interesting feature is to estimate the change of relative Raman intensities between the bending and stretching vibrations of water. As seen in Fig. 2, the peak height of the bending vibration is just about the same as the stretching one when the applied potential is very negative. Even if we considered their integrated Raman intensities, the ratios between the bending and stretching vibrations increase from <0.05 in bulk water[41,50] to 0.1, 0.2, and 0.1 for Ag, Au, and Pt electrodes, respectively. For the physical enhancement of SERS from surface plasmon resonance they should be similar for the two vibrations at a first order approximation, the ratio between the bands due to the bending and stretching vibrations should remain approximately the same as those in the bulk water.[50] Hence, the change in their relative intensity should be from the chemical enhancement effect.

The increase in the relative intensity should be closely associated with the change of the adsorption configuration of interfacial water molecules. In previous works, different interpretations have been suggested. Funtikov and coworkers[50] proposed that this was due to the modulation of the localized

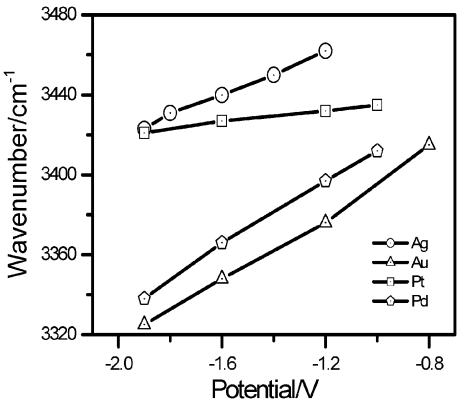

Fig. 3 Vibrational Stark effect for the O–H stretching vibrations in SERS of interfacial water on different materials of electrodes of Ag (circle), Au (triangle), Au@Pt (square), and Au@Pd (pentagon) nanoparticles. The aqueous solution is 0.1 M $NaClO_4$.

surface plasmon resonance on the bending vibration of water at the negative potential. Tian *et al.*[21] suggested that the Raman intensity of the bending vibration is significantly enhanced due to the reorientation of the hydrogen end at the metal surface when the potential is varied at the very negative end of the region of the greatest hydrogen evolution. Chen and Otto[23] proposed that the Raman enhancement of the bending mode was due to the impulse scattering mechanism. Recently, our DFT results on the systems of H_2O–M^- (M = Cu, Ag, Au) showed that the hydrogen bonding interaction between water and metal atomic anions plays an important role, as observed in the aqueous solutions containing halide anions[51,52] or hydrated electrons.[53,54] This will be further analyzed on the basis of the DFT calculations on the negatively charged metallic clusters in the latter section.

Pt–H vibrations

The band at 1984–2009 cm^{-1} shown in Fig. 2 was attributed to the Pt–H vibration, accounting for a full monolayer of top-adsorbed hydrogens on Pt.[55,56] This isotope labeling experimental result confirms that the assignment of the SERS band is correct.[27] The peak at *ca.* 1419 cm^{-1} can be assigned to the stretching of Pt–D. Meanwhile, a peak around 1187 cm^{-1} from D_2O corresponds to the bending vibrational line of normal water ($\sim$1615 cm^{-1}) observed in Fig. 2.

The Pt–H band is very sensitive to applied potential. In previous studies in applied potentials near to the region of the PZC, the Pt–H vibration was observed at about 2090 cm^{-1} by Bewick and coworkers,[57] Tadjeddine and Peremans,[58] and Tian and coworkers[21] on platinum electrodes in acidic aqueous solutions. In the present work, the Pt–H stretching frequency significantly red-shifts from 2009 cm^{-1} at −1.0 V to 1984 cm^{-1} at −1.9 V. The Stark tuning rate was estimated to be about 30 cm^{-1} V^{-1}. On Ag and Au electrodes, no vibrational band can be related to the Ag–H or Au–H bond so far. This is probably due to the relatively weak bonding interaction between hydrogen and silver as well as gold, on which the Tafel mechanism is a much faster step in the HER process.[34]

The pH effect

Fig. 4 presents the SERS spectra of the O–H stretching vibration of water on Au varying with the potential at acidic (pH = 1) and basic (pH = 13) solutions. We first checked the SERS spectra of water at pH = 1. It is significant that by acidifying the solution with $HClO_4$ to pH = 1 one can obtain SERS signals at the more positive potential of −0.4 V, as observed by Funtikov *et al.*[50] This is possibly due to surface species existing in the form of hydrated proton clusters, such as H_3O^+, $H_5O_2^+$, $H_7O_3^+$, or $H_9O_4^+$. In particular, there are two elementary units, Eigen (H_3O^+) and Zundel ($H_5O_2^+$).[59,60] When the negative potential was employed, the hydrated proton clusters interacting with the electrode surface became strong, resulting in the Raman signals of interfacial water emerging at the more positive potential.

It is worth noting that for the acidic solution the Stark tuning rate of the O–H stretching vibration is very small compared to that in the neutral solution (Fig. 5). Tian *et al.* proposed that in acidic solutions water molecules directly adsorbed on electrode surfaces, whereas the hydronium ion was located at least at the second layer.[21] Recently, Olivera *et al.* made a similar conclusion on the basis of their theoretical calculations.[61] They suggested that trihydrated complex ($H_9O_4^+$) adsorbed on a Ag(111) surface had the water molecules located between the hydronium ion and the surface. It is well known that the hydronium cation is not easy to be polarized under the electric field in the double layer. This leads to a small Stark tuning rate compared with that in the neutral solution.

Next we turn to our attention to the basic solution (pH = 13). In contrast to the acidic solution, we can summarize the spectral features of SERS as two points. Firstly, the Stark tuning rate of the O–H stretching vibration is larger at pH = 13 than pH = 1. In the basic solution the surface species is expected to be the hydrated hydroxide ion, the interaction of which with a negatively charged surface is relatively weak due to the electrostatic interaction. Meanwhile, water molecules directly adsorbed on Au become easily polarized. This results in a Stark tuning rate similar to that at pH = 7.

Secondly, the SERS signals are stronger in pH = 13 than pH = 1 and 7 at the same potential. In previous studies, three different mechanisms were suggested to interpret the phenomenon. The first one is that the enhancement originated from an increase of the local electric field in the Helmholtz layer and the reflectivity of Ag electrode surfaces due to the cathodic potential scan.[62] The second suggestion is the adsorption orientation induced enhancement.[21] The third, proposed by Chen and Otto, is the impulse scattering mechanism for the SERS of water.[23] In fact, this can be summed up by the adsorption interaction of different surface species of water clusters on the metal cathode. For three different surface species, such as $H_3O^+(H_2O)_n$, $(H_2O)_n$, and $OH^-(H_2O)_n$, the energies of their first singlet excited states are expected to decrease from the hydrated proton clusters to hydrated hydroxide anionic clusters. This indicates that the hydrated hydroxide anionic clusters should exhibit larger polarizability. Meanwhile, for the metal cathode itself, the concentration of its surface electrons increases with increasing pH, resulting in a

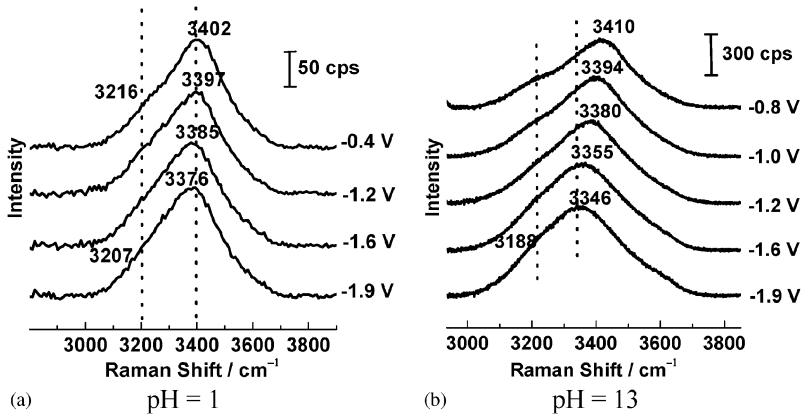

Fig. 4 The pH effect on the O–H stretching frequencies of water adsorbed on the film electrode of gold nanoparticles (a) in 0.1 M $HClO_4$ solution and (b) pH = 13 in the $NaClO_4$ and NaOH solutions.

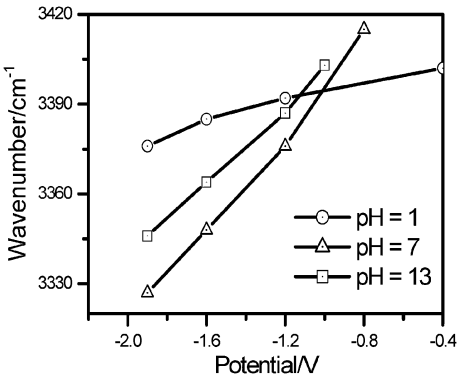

Fig. 5 Vibrational Stark effect for the O–H stretching vibrations in SERS of interfacial water on the film electrode of Au nanoparticles in 0.1 M $NaClO_4$ aqueous solutions with (circle) pH = 1; (triangle) pH = 7, and (square) pH = 13.

larger effective polarizability. The discharge reaction of water on Au obeys the Volmer process, $e + H_2O \rightarrow H_{ad} + OH^-$ in the basic solution.[21,23] The high concentration of the hydroxide ion increases the charge density on electrode surfaces. On the contrary, the interfacial electrons can be scavenged by hydronium ions.[50,63] Therefore, the pH increase results in a decrease of the consumption of electrons on electrode surfaces. Therefore, increasing the pH increases the effective polarizability of surface complexes and further enhances the Raman signals of surface species in the basic solution.

DFT calculations of interfacial water structures

To gain a deeper insight on water adsorbed on the silver, gold, and platinum electrodes, DFT calculations combined with metallic cluster models were carried out using the Gaussian 03 program.[64] Since the experimental potentials were more negative than the PZC potential, the electrode surfaces carry negative charges. This suggests to us a model in which water adsorbs on the metallic cluster by its H-end approaching metal surfaces. The modeling complexes also indicate that the hydrogen bond is formed as O–H···M for silver and gold. For water adsorbed on the Pt electrode, the hydrogen bonding interaction is suggested for water adsorbed on the Pt electrode, *i.e.*, the O–H···H–Pt hydrogen bond. The negative electrode potentials were modeled by negative charges on the metal clusters. A hybrid exchange–correlation functional (B3LYP)[65,66] was used for geometry optimizations and vibrational analysis calculations. For Ag, Au, and Pt atoms, the valence electrons and the internal shells were described by the basis functions, LANL2DZ,[41] and the corresponding relativity effective core potentials, respectively.[67–69] For H and O atoms, we used the augmented triplet-zeta splitting Dunning's correlation consistent basis set with aug-cc-pVTZ.[70,71] The validity of these basis sets has been demonstrated in calculations of a water molecule and its coinage metallic complexes.[72] On top of the optimized geometries, the Raman scattering factors (RSF) of the bending and stretching vibrations of adsorbed water were estimated.

Fig. 6 depicts the optimized structures for a water molecule interacting with Ag_{10}, Au_{10} and a hydrogen covered Pt_{10} cluster, respectively. On these cluster surfaces, the water molecule binding to the clusters adopts a H-down configuration. In contrast to the reported O-down configuration (*i.e.* $H_2O\cdots$H–Pt),[58] our computations surprisingly revealed a H-down configuration (*i.e.* $OH_2\cdots$H–Pt) as the most stable structure of $[H_2O + H_7Pt_{10}]^-$ (Fig. 6c). This is logical since surface adsorbed hydrogens carry negative charges in our model; the water molecules should prefer to approach the surface with its H-end down to take advantage of the hydrogen bonds. Indeed, the same argument applies to Ag and Au surfaces where water molecules directly interact with the electrodes in H-down configurations (*i.e.* $OH_2\cdots$M as in Fig. 6a and b). Experimentally, the oxygen radial distribution function from X-ray measurements on Ag(111) indicated an H-down average orientation of the first layer water at an applied potential about −0.23 V with respect to the PZC.[43]

Upon these interactions, the O–H bond distances in water increased by 0.003–0.006 Å in comparison to those of free water molecules, explaining the red-shift of the O–H stretching frequencies. The optimized bond distances for the $OH_2\cdots$M bond (*i.e.*, between hydrogens of water and the surface metal atoms) were 2.924 Å for H···Ag and 2.961 Å for H···Au, respectively. The optimized H···H distances (*i.e.*, the H-end of water to the surface adsorbed hydrogen) on the Pt cluster were found to be 2.257 Å, within the reported range (1.92–2.48 Å[73]) of the dihydrogen bond distance.

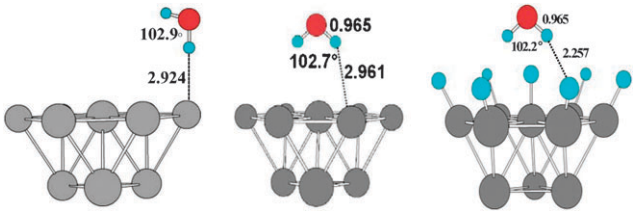

Fig. 6 Optimized structures from cluster models of a water molecule adsorbed on negatively charged metal electrodes, which are mimicked by using Ag_{10}^-, Au_{10}^-, and $Pt_{10}H_7^-$ complexes. (a) $[H_2O + Ag_{10}]^-$; (b) $[H_2O + Au_{10}]^-$; (c) $[H_2O + H_7Pt_{10}]^-$.

The binding energies for a water molecule on the Ag_{10}, Au_{10} and H_7Pt_{10} negatively charged clusters were calculated to be 6.21, 6.71 and 6.03 kcal mol^{-1}, respectively. With increasing applied potential these values are expected to increase. For example, the binding energy for $[Au_{10}H_2O]^{2-}$ increases to 10.17 kcal mol^{-1}. The energies are slightly larger than the water–water interaction energy of a typical hydrogen bond in the bulk water of around 3.69 kcal mol^{-1}[74] and the water–silver interaction energy at the neutral silver.[75] This is also in agreement with the recent theoretical prediction that the water–silver interaction on a charged Ag(111) increases when the negative charge density increases. Although the H···Ag bond distance in the present work is slightly larger than the range of 2.5–2.8 Å reported,[44] we may suppose that on a negatively charged silver surface the most reliable adsorption configuration of water should be by its hydrogen end adjacent to surface metal atoms, through hydrogen bonding.

Note that the dihydrogen bond configuration possibly corresponds to an intermediate of the HER process on Pt. It follows that such a H···H bond as depicted in Fig. 6c plays an important role in HER on electrode surfaces, as it has been reported on some metallorganic and organic systems. Indeed, platinum is always more electropositive than hydrogen in terms of electronegativity, resulting in negatively charged hydrogen adsorbing on its surface. As the electrode potential is moving in the negative region, the $OH_2^{\delta+}\cdots H^{\delta-}$–Pt interaction should enhance the attractive proton–hydride interaction.[73,76] Hence, the present SERS measurement and DFT calculations provide evidence that such a structure on the Pt surfaces may be a stable intermediate of HER in aqueous solutions, as proposed in the Heyrovsky model to account for the slow electrochemical desorption,[34,77] such as in the reaction $H_2O + H(Pt) + e \rightarrow [HO–H\cdots H–Pt]^- \rightarrow HO^- + Pt + H_2$.

Theoretical analysis on Raman intensities

To understand the enhanced Raman signal of the bending vibration of water molecules, it is necessary to discuss the influence of physical and chemical enhancement. Chen and Otto[23] estimated the enhancement factors to be about 10^4-fold for the OH stretching vibration and 10^6-fold for the bending vibration of water on rough silver and copper electrodes. However, smaller enhancement factors were obtained on gold. In our previous report, we suggested an enhancement of the local optical electric field at an adsorbed water molecule on the surface of the metal cluster from the penetration of the surface electronic tail into the solution and the high polarizability of the metal conduction electrons at the more negative potential.[27,78] However, as mentioned in the Introduction, by physical enhancement it is difficult to interpret the specific enhancement of the bending vibration. Also, the effect couldn't directly relate to the adsorption configuration of water molecules at that time.

Now, the results of the DFT calculations presented in Table 2 show that the water molecule interacting through its H-end with a negatively charged metal cluster can result in a larger enhancement in the Raman intensity of the bending vibration than the stretching one. For a free water molecule, the calculated RSF values are 1.0, 101.3, and 26.5 $Å^4$ amu^{-1}, comparable to the experimental data of 0.9 ± 2, 108 ± 14, and 19.2 ± 2.1 $Å^4$ amu^{-1}, respectively.[72,79,80] Accordingly, we may estimate the ratio of differential Raman cross-sections between the bending and symmetric stretching vibrations to be about 0.04 at an excitation line of 632.8 nm. In the neutral water clusters, the ratios are expected to continuously decrease because the Raman scattering factors increase about 2-fold for the bending vibrations and 6-fold for the stretching ones reported in a ring hexamer water cluster.[81]

For water interacting with the negatively charged metal clusters, our calculated results showed that the RSF of the bending vibration was significantly enhanced by one or two orders compared with that of a free water molecule. However, for the O–H stretching vibrations, the biggest RSF magnitude is 2932.5 $Å^4$ amu^{-1} in $[Ag_{10}–H_2O]^-$, which is about 29-fold of the RSF of free water. It is obviously smaller than ~590-fold calculated for the bending vibration. As shown in Table 2, if the experimental excitation wavelength of 632.8 nm was used, we have estimated the ratios of the differential Raman scattering cross-sections (DRSC) between the bending and stretching vibrations to be 0.78, 0.57, and 0.29 for $[Ag_{10}–H_2O]^-$, $[Au_{10}–H_2O]^-$, and $[Pt_{10}H_7–H_2O]^-$, respectively. Increasing the

Table 2 Calculated frequencies (cm^{-1}), scattering factors (S_R, $Å^4$ amu^{-1}) and differential Raman scattering cross-sections (I_R, cm^2 $mole^{-1}$ rad^{-1}), and Raman intensity ratios of bending and stretching bands (I_b/I_v) of intramolecular vibrations in free water and water interacting with negatively charged metal clusters

Species	Frequency	Scaled frequency[a]	S_R	I_R[b]	I_b/I_v
H_2O	1627.4	1596.5	1.0	0.01	
	3796.4	3655.9	101.3	0.35	0.04
	3899.0	3754.7	26.5	0.09	
$[Ag_{10}–H_2O]^-$	1636.8	1605.7	592.1	8.75	
	3624.9	3490.8	2932.5	11.27	0.78
	3836.8	3694.8	273.8	0.93	
$[Au_{10}–H_2O]^-$	1640.2	1609.0	29.1	0.43	
	3751.7	3612.9	209.4	0.75	0.57
	3831.3	3689.5	80.9	0.28	
$[Au_{10}–H_2O]^{2-}$	1657.5	1626.0	201.8	2.93	
	3692.6	3556.0	277.5	1.03	2.86
	3800.9	3660.3	22.5	0.08	
$[Pt_{10}H_7–H_2O]^-$	1652.8	1621.4	16.1	0.23	
	3744.2	3605.7	224.2	0.80	0.29
	3814.1	3673.0	3.5	0.01	

[a] The factors of 0.981 and 0.963 extracted from the previous work (ref. 72) at the same theoretical level were used to scale the theoretical vibrational frequencies of the bending and stretching modes of free water and adsorbed water. [b] Differential Raman scattering cross-sections were calculated at the excitation wavelength of 632.8 nm.

negative charge to −2 for Au_{10} leads to the Raman scattering factors of the bending vibration comparable to the stretching vibration. Meanwhile, an unexpected DRSC ratio of 2.86 was obtained. Although it is too large to doubt its reliability, it indicates that the bending vibration is very sensitive to the surface charge density of the electrode surface in the hydrogen bonded configuration.

This makes us realize that the change in the relative intensities of intramolecular bending and stretching vibrations for water is very possibly an indicator of the H-down configuration of water adsorbed on electrode surfaces. Although adsorption configurations were suggested for the interfacial waters in many previous studies,[21,23,50] the present results propose that the changes of the relative Raman intensities are closely associated with the hydrogen bonding of the interfacial water molecules to metal electrode surfaces. In our recent paper, this is interpreted by the vibrational coupling of the bending mode of adsorbed water with the hydrogen bond.[72] The enhancement in the Raman intensities of the bending vibrations of the interfacial water molecules can be considered as an indicator that the water is binding to metal atoms through its H-end.

Fig. 7 shows simulated Raman spectra of a water molecule interacting with a gold atom (Au), a gold atomic anion (Au^-), Au_{10}^-, and Au_{10}^{2-}. In our previous work, the most stable structures predicted at the same theoretical level are the oxygen atom of water binding to the gold atom in the neutral species and a hydrogen atom binding to the gold atom in the anionic one.[72] The calculated Raman scattering factors of their bending and intense stretching vibrations are 3.7 and 235.0 $Å^4$ amu^{-1} for H_2O–Au, and 130.8 and 454.4 $Å^4$ amu^{-1} for $[H_2O–Au]^-$. The peaks corresponding to the bending vibration shown in Fig. 7 depend strongly on the adsorption configuration and the charge amount. Fig. 7a shows that the relative Raman intensity in H_2O–Au is very similar to that of water in the gas phase or a pure liquid. However, applying a negative charge to H_2O–Au results in a significant enhancement in the Raman intensity of the bending vibration in $[H_2O–Au]^-$ (Fig. 7b). For negatively charged Au_{10} clusters, the relative intensity of the bending vibration is significantly enhanced from $[Au_{10}–H_2O]^-$ (Fig. 7c) to $[Au_{10}–H_2O]^{2-}$(Fig. 7d).

Interfacial water models on metal cathodes

Three interesting features have been observed from the potential-dependent SERS spectra of water on these metal cathodes. First, the OH stretching frequency exhibits a metal-dependent property. The Stark tuning rate for Pt is the smallest. Second, the Raman signal of the bending vibration of adsorbed water is significantly enhanced compared to that of its stretching vibration when applied potentials move negatively. Third, the SERS spectra are very sensitive to the pH value. Accordingly, we propose two adsorption models for the three metal cathodes in Fig. 8.

Fig. 8a depicts the interfacial water structure on the Pt cathode. In the case, the interfacial water molecules adsorb at the second layer while the first adsorption layer is hydrogen. This was proposed mainly from the observation that the very small Stark tuning rate on Pt was obtained. Further evidence that supports this picture is that the Raman band observed at *ca.* 2000 cm^{-1} is related to the Pt–H stretching vibration. Previous studies indicated that chemically adsorbed hydrogen atoms were only observed at a potential where the coverage of adsorbed hydrogens reaches a full monolayer on the platinum electrode.[55,56] The present model confirms the previous conclusion.

We note that it is difficult to infer the orientation of the second-layer water molecules from the above experimental result. Water molecules adsorbed on platinum electrodes were extensively investigated, experimentally and theoretically.[57,58,82,83] However, the studied systems were generally limited to water adsorption directly on a platinum surface or only at a potential region of lesser HERs. On the basis of the sum-frequency generation spectra, Tedjeddine *et al.* proposed that the interfacial water molecule interacts with surface hydrogens through hydrogen bonds by its oxygen atom.[58] As plotted in Fig. 8a, we have proposed that the water molecules interact with chemically adsorbed hydrogen atoms through the hydrogen bond of their hydrogen ends in DFT calculations.

The model presented in Fig. 8b shows that the hydrogen atoms of interfacial water molecules directly bind to electrode surfaces. This leads to a larger Stark tuning rate. According to the adsorption model, the frequency shifts of water on Ag and Au should be sensitive to potential variation, which agrees with our experimental results and the work in the literature.[27,43] Therefore, it is possible that the water molecule may bind to surfaces through one or two hydrogen atoms, depending on the applied potentials and the properties of the electrode materials. On one hand, the model can interpret the red shift of the OH stretching frequency with negative-moving potential. On the other hand, combined with DFT calculations, this can explain why the SERS intensities of the bending mode of water are selectively enhanced with the negatively moving electrode potential.

Conclusion

We have successfully observed the SERS spectra of interfacial water on metal film cathodes of silver, gold, and platinum nanoparticles at very negative applied potentials. The Raman signal and noise ratios recorded from the nanoparticle electrodes are obviously better than those reported from the bulk electrodes in previous works. Using the high electromagnetic enhancement of the Au core to effectively boost the surface Raman signal on the shell metals, we have successfully observed the SERS signals of surface water and adsorbed hydrogen atoms on the platinum metal at the same time. SERS measurement also demonstrated that the spectroscopy technique can be used to study probed molecules with a low Raman scattering cross section adsorbed on weakly SERS-active materials boosted by utilizing core–shell nanoparticles.

By inspecting the variation of the peak positions with applied potentials, it was found that different vibrational Stark effects were observed on these metal electrodes, indicating that there exists spectroelectrochemical properties dependent on the metal materials. On the basis of the SERS results, combined with DFT calculations, we propose conceptual

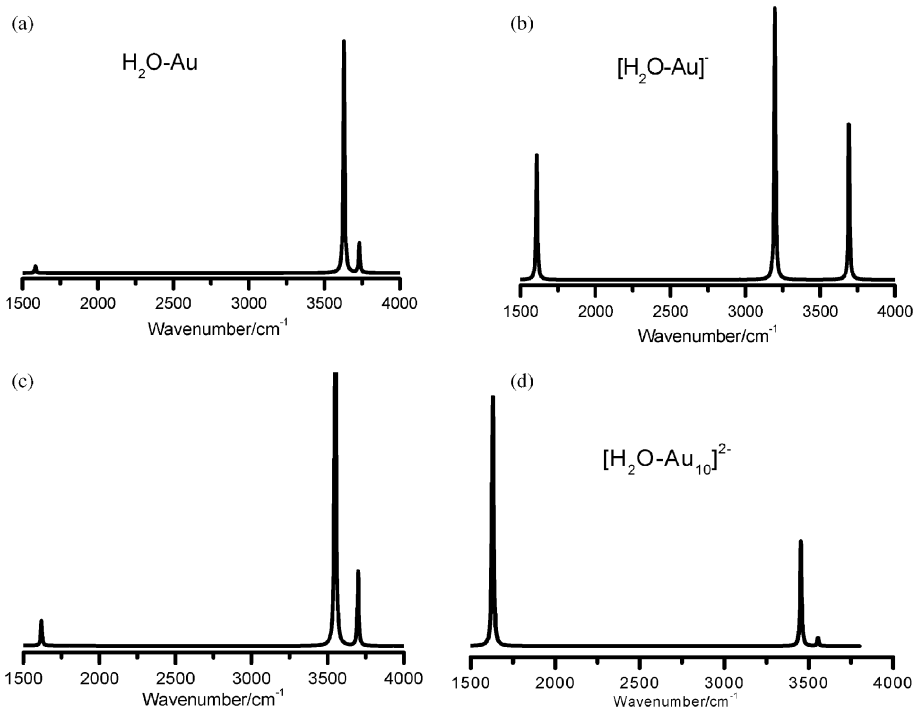

Fig. 7 Theoretical simulation Raman spectra of (a) H_2O–Au; (b) $[H_2O–Au]^-$; (c) $[H_2O–Au_{10}]^-$; and (d) $[H_2O–Au_{10}]^{2-}$ complexes. The parameters used are 632.8 nm for the excitation wavelength and 20 cm^{-1} for the half-width at the half maximum height.

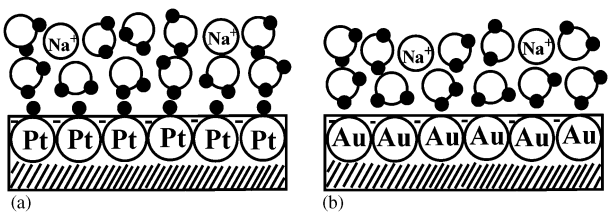

Fig. 8 Proposed models for interfacial water molecules adsorbed on film electrodes of (a) platinum and (b) gold (silver) nanoparticles at a potential very negative to their potential of hydrogen evolution reaction.

models for water adsorbed on the three metal surfaces. For silver and gold electrodes, interfacial water molecules directly interact with the electrodes through the hydrogen bond of their hydrogen atoms contacting electrode surfaces carrying negative charges due to cathodic polarization. For the platinum cathode interfacial water molecules adsorb at the second layer while the first layer species are a full monolayer of adsorbed hydrogen atoms. The results of DFT calculations allow us to propose that water molecules at the second layer interact with the platinum cathode through the dihydrogen bonds in a H-down configuration.

The present study also showed that the combined results of SERS and DFT correlated the adsorption structure of the interfacial water with the specific enhancement of the bending vibration of adsorbed water molecules. We believe that surface vibrational spectroscopy will become an increasingly general and indispensable tool in fundamental and applied studies for interfacial structures and processes involving water molecules.

Acknowledgements

We thank the financial support of this work by the NSF of China (grant Nos 20433040, 20573087, 20973143) and National Basic Research Program of China (973 Program 2007CB815303 and 2009CB930703). DYW thanks the financial support from NCETFJ, J0630429 and HPC of Xiamen University.

References and notes

1 A. M. Kuznetsov and J. Ulstrup, *Electrochim. Acta*, 2000, **45**, 2339–2361.
2 R. Parsons, *Chem. Rev.*, 1990, **90**, 813.
3 G. Merga, L. C. Cass, D. M. Chipman and D. Meisel, *J. Am. Chem. Soc.*, 2008, **130**, 7067–7076.
4 M. Ito, *Surf. Sci. Rep.*, 2008, **63**, 329–389.
5 J. O. M. Bockris and S. U. M. Khan, *Quantum Electrochemistry*, Plenum, New York, 1979.
6 *Topics in Applied Physics*, ed. K. Wandelt and S. Thurgate, Springer, Berlin, 2003.
7 A. K. Bewick and Keiji, *Surf. Sci.*, 1980, **101**, 131.
8 M. Osawa, *Bull. Chem. Soc. Jpn.*, 1997, **70**, 2861–2880.
9 A. P. Tadjeddine, A., *J. Electroanal. Chem.*, 1996, **409**, 115.
10 Z. D. Schultz, S. K. Shaw and A. A. Gewirth, *J. Am. Chem. Soc.*, 2005, **127**, 15916–15922.
11 H. Noguchi, T. Okada and K. Uosaki, *Electrochim. Acta*, 2008, **53**, 6841–6844.
12 S. Nihonyanagi, Y. Shen, K. Uosaki, L. Dreesen, C. Humbert, P. Thiry and A. Peremans, *Surf. Sci.*, 2004, **573**, 11–16.
13 M. Osawa, M. Tsushima, H. Mogami, G. Samjeske and A. Yamakata, *J. Phys. Chem. C*, 2008, **112**, 4248–4256.
14 M. Futamata, L. Q. Luo and C. Nishihara, *Surf. Sci.*, 2005, **590**, 196–211.
15 M. Futamata, *J. Electroanal. Chem.*, 2003, **550–551**, 93–103.
16 M. Fleischmann, P. J. Hendra, I. R. Hill and M. E. Pemble, *J. Electroanal. Chem.*, 1981, **117**, 243.

17 B. Pettinger, M. R. Philpott and J. G. Gordon, *J. Chem. Phys.*, 1981, **74**, 934–940.
18 T. T. O. Chen, J. F., R. K. Chang and B. L. Laube, *Chem. Phys. Lett.*, 1982, **89**, 356–361.
19 S. H. F. Macomber, T. E. and T. M. Devine, *Chem. Phys. Lett.*, 1982, **90**, 439–444.
20 J. F. C. Owen and R. K., *Chem. Phys. Lett.*, 1984, **104**, 510–515.
21 Z. Q. Tian, B. Ren, Y. X. Chen, S. Z. Zou and B. W. Mao, *J. Chem. Soc., Faraday Trans.*, 1996, **92**, 3829–3838.
22 Y. X. Chen, S. Z. Zou, K. Q. Huang and Z. Q. Tian, *J. Raman Spectrosc.*, 1998, **29**, 749–756.
23 Y. X. Chen and A. Otto, *J. Raman Spectrosc.*, 2005, **36**, 736–747.
24 M. H. Fleischmann, P. J. and A. J. McQuillan, *Chem. Phys. Lett.*, 1974, **26**, 163–166.
25 D. L. Jeanmaire and R. P. Van Duyne, *J. Electroanal. Chem.*, 1977, **84**, 1–20.
26 M. G. C. Albrecht and J. Alan, *J. Am. Chem. Soc.*, 1977, **99**, 5215–5217.
27 Y. X. Jiang, J. F. Li, D. Y. Wu, Z. L. Yang, B. Ren, J. W. Hu, Y. L. Chow and Z. Q. Tian, *Chem. Commun.*, 2007, 4608–4610.
28 Z. Q. Tian, B. Ren and D. Y. Wu, *J. Phys. Chem. B*, 2002, **106**, 9463–9483.
29 Z. Q. Tian and B. Ren, *Annu. Rev. Phys. Chem.*, 2004, **55**, 197–229.
30 Z. Q. Tian, B. Ren, J. F. Li and Z. L. Yang, *Chem. Commun.*, 2007, 3514–3534.
31 M. T. M. Koper and R. A. van Santen, *J. Electroanal. Chem.*, 1999, **472**, 126–136.
32 G. Frens, *Nat. Phys. Sci.*, 1973, **241**, 20–22.
33 S. Trasatti, *Surf. Sci.*, 1995, **335**, 1.
34 J. O. M. Bockris and S. U. M. Khan, *Surface Electrochemistry—A Molecular Level Approach*, Plenum, New York, 1993.
35 M. Perner, P. Bost, U. Lemmer, G. von Plessen, J. Feldmann, U. Becker, M. Mennig, M. Schmitt and H. Schmidt, *Phys. Rev. Lett.*, 1997, **78**, 2192.
36 C. Sonnichsen, T. Franzl, T. Wilk, G. von Plessen, J. Feldmann, O. Wilson and P. Mulvaney, *Phys. Rev. Lett.*, 2002, **88**, 077402.
37 A. Otto, I. Mrozek, H. Grabhorn and W. Akemann, *J. Phys.: Condens. Matter*, 1992, **4**, 1143–1212.
38 M. Futamata, *Isr. J. Chem.*, 2006, **46**, 265–281.
39 M. Moskovits and K. H. Michaelian, *J. Chem. Phys.*, 1978, **69**, 2306–2311.
40 P. Hobza and Z. Havlas, *Chem. Rev.*, 2000, **100**, 4253–4264.
41 D. Eisenberg and W. Kauzmann, *The Structure and Properties of Water*, Oxford University, London, 1969.
42 S. V. Shirin, O. L. Polyansky, N. F. Zobov, R. I. Ovsyannikov, A. G. Csaszar and J. Tennyson, *J. Mol. Spectrosc.*, 2006, **236**, 216.
43 M. F. Toney, J. N. Howard, J. Richer, G. L. Borges, J. G. Gordon, O. R. Melroy, D. G. Wiesler, D. Yee and L. B. Sorensen, *Nature*, 1994, **368**, 444.
44 C. G. Sanchez, *Surf. Sci.*, 2003, **527**, 1–11.
45 H. Ogasawara, B. Brena, D. Nordlund, M. Nyberg, A. Pelmenschikov, L. G. M. Pettersson and A. Nilsson, *Phys. Rev. Lett.*, 2002, **89**, 276102.
46 K. Morgenstern and J. Nieminen, *Phys. Rev. Lett.*, 2002, **88**, 066102.
47 R. Ludwig, *Angew. Chem., Int. Ed.*, 2003, **42**, 3458–3460.
48 G. E. Walrafen and L. A. Blatz, *J. Chem. Phys.*, 1973, **59**, 2646.
49 M. Futamata, *Surf. Sci.*, 1999, **427–428**, 179–183.
50 A. M. Funtikov, S. K. Sigalaev and V. E. Kazarinov, *J. Electroanal. Chem.*, 1987, **228**, 197–218.
51 W. R. Busing and D. F. Hornig, *J. Phys. Chem.*, 1961, **65**, 284.
52 J. W. Schultz and D. F. Hornig, *J. Phys. Chem.*, 1961, **65**, 2131.
53 M. J. Tauber and R. A. Mathies, *Chem. Phys. Lett.*, 2002, **354**, 518–526.
54 M. Mizuno and T. Tahara, *J. Phys. Chem. A*, 2003, **107**, 2411–2421.
55 B. Ren, X. Xu, X. Q. Li, W. B. Cai and Z. Q. Tian, *Surf. Sci.*, 1999, **427–428**, 157–161.
56 X. Xu, D. Y. Wu, B. Ren, H. Xian and Z. Q. Tian, *Chem. Phys. Lett.*, 1999, **311**, 193–201.
57 A. R. Bewick and J. W., *J. Electroanal. Chem.*, 1982, **132**, 329.
58 A. Peremans and A. Tadjeddine, *Phys. Rev. Lett.*, 1994, **73**, 3010–3013.
59 M. Eigen and L. D. Maeyer, *Proc. R. Soc. London, Ser. A*, 1958, **247**, 505.
60 G. Zundel and H. Metzer, *Z. Phys. Chem.*, 1968, **58**, 225.
61 P. P. Olivera, A. Ferral and E. M. Patrito, *J. Phys. Chem. B*, 2001, **105**, 7227–7238.
62 T. Itoh, Y. Sasaki, T. Maeda and C. Horie, *Surf. Sci.*, 1997, **389**, 212–222.
63 H. A. Schwartz, *J. Phys. Chem.*, 1992, **96**, 8937–8941.
64 M. J. Frisch, G. W. Trucks, H. B. Schlegel, G. E. Scuseria, M. A. Robb, J. R. Cheeseman, J. A. Montgomery, Jr., T. Vreven, K. N. Kudin, J. C. Burant, J. M. Millam, S. S. Iyengar, J. Tomasi, V. Barone, B. Mennucci, M. Cossi, G. Scalmani, N. Rega, G. A. Petersson, H. Nakatsuji, M. Hada, M. Ehara, K. Toyota, R. Fukuda, J. Hasegawa, M. Ishida, T. Nakajima, Y. Honda, O. Kitao, H. Nakai, M. Klene, X. Li, J. E. Knox, H. P. Hratchian, J. B. Cross, V. Bakken, C. Adamo, J. Jaramillo, R. Gomperts, R. E. Stratmann, O. Yazyev, A. J. Austin, R. Cammi, C. Pomelli, J. Ochterski, P. Y. Ayala, K. Morokuma, G. A. Voth, P. Salvador, J. J. Dannenberg, V. G. Zakrzewski, S. Dapprich, A. D. Daniels, M. C. Strain, O. Farkas, D. K. Malick, A. D. Rabuck, K. Raghavachari, J. B. Foresman, J. V. Ortiz, Q. Cui, A. G. Baboul, S. Clifford, J. Cioslowski, B. B. Stefanov, G. Liu, A. Liashenko, P. Piskorz, I. Komaromi, R. L. Martin, D. J. Fox, T. Keith, M. A. Al-Laham, C. Y. Peng, A. Nanayakkara, M. Challacombe, P. M. W. Gill, B. G. Johnson, W. Chen, M. W. Wong, C. Gonzalez and J. A. Pople, *GAUSSIAN 03*, Gaussian, Inc., Wallingford, CT, 2004.
65 A. D. Becke, *J. Chem. Phys.*, 1993, **98**, 5648.
66 C. Lee, W. Yang and R. G. Parr, *Phys. Rev. B: Condens. Matter*, 1988, **37**, 785.
67 P. J. Hay and W. R. Wadt, *J. Chem. Phys.*, 1985, **82**, 270.
68 W. R. Wadt and P. J. Hay, *J. Chem. Phys.*, 1985, **82**, 284.
69 P. J. Hay and W. R. Wadt, *J. Chem. Phys.*, 1985, **82**, 299.
70 J. T. H. Dunning, *J. Chem. Phys.*, 1989, **90**, 1007.
71 R. A. Kendall, T. H. Dunning, Jr. and R. J. Harrison, *J. Chem. Phys.*, 1992, **96**, 6796.
72 D. Y. Wu, S. Duani, X. M. Liu, Y. C. Xu, Y. X. Jiang, B. Ren, X. Xu, S. H. Lin and Z. Q. Tian, *J. Phys. Chem. A*, 2008, **112**, 1313–1321.
73 M. J. Calhorda, *Chem. Commun.*, 2000, 801–809.
74 A. Rahman and F. H. Stilinger, *J. Chem. Phys.*, 1974, **60**, 154.
75 V. A. Ranea, A. Michaelides, R. Ramirez, J. A. Verges, P. L. de Andres and D. A. King, *Phys. Rev. B: Condens. Matter Mater. Phys.*, 2004, **69**, 205411.
76 R. H. Crabtree, *Science*, 1998, **282**, 2000–2001.
77 J. O. M Bockris and K. S. U. M., *Surface Electrochemistry—A Molecular Level Approach*, Plenum, New York, 1993.
78 B. I. Lundqvist, O. Gunnarsson, H. Hjelmberg and J. K. Norskov, *Surf. Sci.*, 1979, **89**, 196–225.
79 W. F. Murphy, *Mol. Phys.*, 1977, **33**, 1701.
80 W. F. Murphy, *Mol. Phys.*, 1978, **36**, 727.
81 H. Cybulski and J. Sadlej, *Chem. Phys.*, 2007, **342**, 163–172.
82 K. Kunimatsu, T. Senzaki, G. Samjeske, M. Tsushima and M. Osawa, *Electrochim. Acta*, 2007, **52**, 5715–5724.
83 M. Nakamura, H. Kato and N. Hoshi, *J. Phys. Chem. C*, 2008, **112**, 9458–9463.

